Investigation of C-A-S-H composition, morphology and density in Limestone Calcined Clay Cement (LC^3)

François Avet*, Emmanuelle Boehm-Courjault, Karen Scrivener

Laboratory of Construction Materials, IMX, EPFL, 1015 Lausanne, Switzerland

A B S T R A C T

In this study, the C-A-S-H composition, morphology and density are characterized for Limestone Calcined Clay Cement (LC^3-50) blends containing clays with various kaolinite contents. Significant incorporation of aluminium is observed for LC^3-50 blends compared with reference Portland cement (PC), and this incorporation increases with the kaolinite content of the calcined clay. No change of C-A-S-H morphology was observed by Transmission Electron Microscopy (TEM) between reference PC and LC^3-50 blends, with a "fibrillar" morphology for all samples. The determination of the density of C-A-S-H measured by ^{1}H NMR also shows very similar results with a bulk density close to 2.0 g·cm^{-3} and a solid density of around 2.8 g·cm^{-3} for all systems.

1. Introduction

C-S-H is the main hydrated phase present in Portland cement based cementitious materials. The solid structure of C-S-H, based on tobermorite, is composed of a complex layer of Ca and O atoms in contact on both sides with silica chains. The silica chains show a dreierketten arrangement with two silica tetrahedra pairing the calcium oxide layers and a third bridging to the next pair of silicates [1,2]. The space between the layers of calcium oxide and silicate chains is the interlayer space which is mainly composed of water and calcium ions. C-S-H has a variable stoichiometric composition depending of the pore solution concentration, which is in turn affected by factors such as the water to binder ratio [3], clinker composition [4] and mix composition [5–9]. C-S-Hs found in cementitious materials have higher calcium to silicon ratios than tobermorite in the range of 1.3–2 [10–13]. Three kinds of defects allow for the variation in calcium to silicon ratio: missing bridging silicate tetrahedra; substitution of two protons terminating unlinked silicate tetrahedra by calcium ions; and calcium ions in the interlayer [14–16]. Ions other than silicon and calcium can be found in C-S-H. The most common one is aluminium, which mostly occupies bridging sites linking dimers of silicate tetrahedra [1,17–19] and which may lead to an increase of the average chain length of C-S-H [20]. The term C-A-S-H is often used rather than C-S-H to take account of the aluminium incorporation. Higher aluminium contents in C-A-S-H are usually observed with alumino silicate SCMs: slags, fly ash and especially calcined clays [4,6,7,21].

Measurement of the C-A-S-H composition by SEM-EDS is challenging for blends containing fine particles such as metakaolin or silica fume due to the volume of interaction of the electron beam with the sample. This interaction volume can include C-A-S-H and also other phases. Transmission Electron Microscopy in scanning mode (STEM) provides a complementary tool to estimate the C-A-S-H composition free of interaction with other phases [22]. STEM also gives more information on the C-A-S-H morphology. Richardson [23] has reported "fibrillar-like" or "foil-like" morphologies for outer C-A-S-H, with a foil-like morphology only observed for Ca/Si atomic ratios at or below 1.5. A more compact uniform morphology is observed for inner products.

New insights on C-A-S-H are provided by the use of ^{1}H Nuclear Magnetic Resonance (^{1}H NMR) relaxometry. This method allows measurement of the water in the interlayer and gel pores of the C-A-S-H, as shown by Muller et al. [24,25]. This technique is non-destructive and does not require any drying prior to analysis. Continuous measurements can be carried out to track the evolution of the different water populations with time. Müller used these data for a mass and volume balance to determine the density of both solid (excluding gel water) and bulk (including get water) of the C-A-S-H [24].

These two techniques are used here to characterize the C-A-S-H in Limestone Calcined Clay Cements (LC^3).[1]

We previously showed that for LC^3-50 systems with a clinker content of only 50%, similar strength to reference PC is obtained from 7 days onwards even using clays with a calcined kaolinite content as low as 40% [26]. SEM-EDS indicated a wide range of compositions for the C-A-S-H in these blends. Here, the composition, the morphology and the density of C-A-S-H were studied for LC^3-50 blends using a wide range of calcined kaolinitic clays and the results are compared with plain PC. The chemical composition of the C-A-S-H was determined

---

* Corresponding author.

E-mail address: francois.avet@epfl.ch (F. Avet).

[1] LC^3: Limestone Calcined Clay Cement: http://www.lc3.ch.

using both SEM-EDS and STEM-EDS techniques. STEM was also used to investigate the influence of the calcined kaolinite content on the morphology of C-A-S-H. The density of C-A-S-H was obtained based on ^{1}H NMR results. Moreover, thanks to the valuable information provided by ^{1}H NMR [27], especially concerning the amount of gel and capillary water, a precise characterization of the porosity of these cementitious materials is obtained. The porosity of LC^3-50 was investigated and the results compared with reference cement to give a better understanding of the results obtained with the widely-used Mercury Intrusion Porosimetry (MIP) technique.

2. Materials characteristics and mix design

This study looks at similar systems to those reported in [26] in which a commercial CEMI 42.5R grey cement from Heidelberg cement was used. The same cement was used for study of the morphology and the composition of the C-A-S-H. In addition to reference PC, LC^3-50 systems were studied, in which 45 parts of cement are substituted by 30 parts of calcined clays and 15 parts of limestone. The cement used is properly sulfated for a plain PC hydration, but 2% of gypsum needs to be added to prevent undersulfation for LC^3-50 blends [26]. The optimal sulfate addition was obtained when it was possible to observe a clear separation between the silicate and aluminate peak on the heat flow curves by isothermal calorimetry. A gypsum from Acros (98+ grade) was used.

Due to the complexity of preparing the samples for TEM, this was only done for three calcined clays in LC^3-50 blends, in addition to plain PC. The kaolinite content was determined by Thermogravimetric Analysis (TGA) and the calcined kaolinite content is defined as the difference between the kaolinite content before and after calcination. The final mix designs are shown in Table 1.

For the determination of C-A-S-H density, the use of this grey cement was not compatible with ^{1}H NMR measurements. The iron content (3.6% Fe_2O_3) is too-high decreasing the magnetization and degrading the accuracy of the results [28]. Thus, a white cement from Aalborg Cement was used for all ^{1}H NMR experiments. Plain white cement (WPC) and LC^3 blends (WLC^3-50) were cast.

The alkali level of the white cement was adjusted in order to get similar Na_2O_{eq} to the grey cement used in the previous studies. Potassium hydroxide (Acros) was used for the alkali adjustment.

The sulfate level was also adjusted based on heat flow curves by isothermal calorimetry. 2% of gypsum was added for WPC and 3% for WLC^3-50 blends.

Since many kaolinitic clays contain significant amount of iron oxide, some simulated mixes of fairly pure kaolinitic clay with quartz were used. In addition to WLC^3-50 with 95.0% of calcined kaolinite, two mixes were prepared by replacing 50% and 75% of calcined clay by quartz to model calcined clays with 23.8% and 47.5% of calcined kaolinite, respectively. A fourth blend consisted of a clay with a low iron oxide content (1.0%) and 39.0% of calcined kaolinite. The final mix compositions used for the determination of C-A-S-H density is shown in Table 2.

The XRF and the physical characteristics of the grey and white cements, the limestone, and the different calcined clays are shown in Table 3.

3. Analytical details

3.1. C-A-S-H morphology and composition

The PC and the LC^3-50 (17.0%), (50.3%) and (95.0%) were examined after 28 days of hydration. A similar protocol to that detailed in [4] was used for the sample preparation. The paste was mixed for 2 min at 1600 rpm. Slices were cut at 28 days of hydration. Hydration was stopped using solvent exchange method (isopropanol). This method is the best for preserving the microstructure [29,30]. The slices were then stored in a desiccator under vacuum. For TEM samples, a small piece of paste was impregnated in a hard resin (Gatan G2) and the impregnated sample was cut as a $2 \times 2 \times 0.7$-mm^3-slice using a diamond saw. This slice is then polished using diamond-lapping films (Allied) until optical translucency. Due to the brittleness of hydrated cementitious paste, it is not possible to get a uniform thin lamella. Thin areas could be obtained only using the Tripod method at the edge of a bevel. The last step of polishing is done by ion milling (Gatan 691) using Precision Ion Polishing System (PIPS) until reaching electron transparency (thickness of about 100–150 nm). Low voltages of 1–2 kV were used in order to avoid ion beam damage. The detection of fringes of equal thickness by optical microscopy is a good indication of the presence of areas transparent to electrons.

For the SEM sample preparation, a quarter of a slice was impregnated in epoxy resin (Epotek-301) and the impregnated sample was then polished with diamond particles of 9 μm, 3 μm and 1 μm for 30 min, 2 h and 3 h, respectively.

For the TEM observations, a FEI Tecnai Osiris was used (CIME, EPFL) with a XFEG source. Two Super-X Windowless SDD EDS detectors were used. Both the Bright Field (BF) and the High Angle Annular Dark Field (HAADF) detectors were used in scanning mode (STEM). An acceleration voltage of 80 kV (combined with small spot size) was used in order to avoid beam damage. A magnification of 56,000× for imaging was used.

Once the images were taken, several zones of interest were delimited and analysed to get their global EDS spectrum. Between 5 and 15 areas were analysed to get the C-A-S-H composition. The C-A-S-H composition obtained by STEM-EDS was compared with results obtained by SEM-EDS. The determination of the C-A-S-H composition was done according to the method of Rossen [4]. An FEI Quanta 200 SEM was used with an accelerating voltage of 15 kV, with a working distance of 12.5 mm, and a spot size adjusted to get a current of approximately 0.8 nA. The determination of C-A-S-H composition was obtained from 200 points per sample. In order to get a more accurate composition of C-A-S-H, inner product areas were sampled to minimise intermixing with other phases present in the microstructure.

3.2. C-A-S-H density

Immediately after mixing for 2 min at 1600 rpm, about 0.5 g of fresh paste was put into a tube for NMR experiments. The tube was then sealed with parafilm and directly inserted in the NMR device to be continuously tested. A Bruker Minispec NMR spectrometer was used for all experiments. The temperature of the device was kept constant at 20 °C. Both Carr-Purcell-Meiboom-Gill (CPMG) and Quadrature-Echo (QE) pulse sequences were carried out in order to cover the whole range of relaxation times. The CPMG and QE pulse sequences were alternately used in a 3 hour/ 1 hour arrangement. For QE sequences, the pulse gap τ was varied from 15 μs to 45 μs. The signal was decomposed into the Gaussian solid part and the exponential liquid part. The solid intensity was then extrapolated to zero pulse using a Gaussian fit. Concerning the liquid part, the CPMG sequence was composed of 256 echoes recorded from 50 μs to 12 ms in a logarithmic spacing to cover five ranges of relaxation times. From the echo decays, the Inverse Laplace Transform

Table 1

Mix composition of PC and LC^3-50 blends. The brackets indicate the calcined kaolinite content of the calcined clay for LC^3-50 blends.

Composition (%)	Cement		Calcined clay	Limestone	Gypsum addition
	Clinker	Anhydrite			
PC	94.1	5.9	–	–	–
LC^3-50 (17.0%)	50.6	3.3	29.4 (17.0%)	14.7	2.0
LC^3-50 (50.3%)	50.6	3.3	29.4 (50.3%)	14.7	2.0
LC^3-50 (95.0%)	50.6	3.3	29.4 (95.0%)	14.7	2.0

Table 2

Mix composition of WPC and WLC³-50 blends. The brackets indicate the calcined kaolinite content of the calcined clay for each WLC³-50 mix.

%	Cement		Calcined clay	Quartz	Limestone	Alkali addition	Gypsum addition
	Clinker	Gypsum					
WPC	92.7	4.2	–	–	–	1.2	2.0
WLC³-50 (95.0%)	50.7	2.3	28.9 (95.0%)	–	14.5	0.6	3.0
WLC³-50 (47.5%)	50.7	2.3	14.5 (95.0%)	14.5	14.5	0.6	3.0
WLC³-50 (39.0%)	50.7	2.3	28.9 (39.0%)	–	14.5	0.6	3.0
WLC³-50 (23.8%)	50.7	2.3	7.2 (95.0%)	21.7	14.5	0.6	3.0

Table 3

XRF composition and physical properties of white cement, calcined clays and limestone.

	Calcined clays				Quartz	Grey cement	White Cement	Limestone
Calcined kaolinite content (%)	17.0	50.3	95.0	39.0	0	–	–	–
$D_{v,50}$ (μm)	5.9	10.9	5.1	10.8	11.2	8.4	7.4	7.2
BET specific surface (m²/g)	18.7	45.7	9.6	10.7	1.2	0.9	1.3	1.8
SiO_2	68.4	44.9	52.0	71.0	99.8	19.3	24.2	0.1
Al_2O_3	17.5	32.3	43.8	23.4	–	5.7	1.9	–
Fe_2O_3	8.9	15.4	0.3	1.0	–	3.6	0.3	–
CaO	0.6	1.3	–	0.3	–	63.6	69.2	55.0
MgO	0.7	0.8	–	0.4	–	1.6	0.7	0.2
SO_3	–	0.1	0.1	–	–	3.2	2.0	–
Na_2O	0.1	0.4	0.3	0.2	–	0.2	0.2	0.1
K_2O	2.3	0.2	0.1	1.4	0.1	1.2	0.1	–
TiO_2	0.8	2.4	1.5	1.2	–	0.3	0.1	–
P_2O_5	0.1	0.4	0.2	0.2	–	0.2	0.3	–
MnO	0.1	0.1	–	–	–	0.1	–	–
Others	0.2	0.2	0.1	–	–	0.3	0.3	–
LOI	0.5	1.7	1.5	0.9	0.1	0.8	0.9	42.6

(ILT) was applied to extract the relaxation times. The regularization factor which sets the sensitivity of the ILT is set to 1.5×10^{-6}.

The methodology for the determination of the C-A-S-H density by ¹H NMR is provided as Supplementary material. Mass and volume balances are applied, and in addition to ¹H NMR outputs, other data are required, such as the clinker, limestone and metakaolin reaction degree, as well as the chemical shrinkage data.

For the XRD data needed for the mass and volume balance, the tests were carried out on fresh slices at 1, 3, 7, 28 and 90 days of hydration. XRD patterns were acquired with Bragg-Brentano mode with a X'Pert PANalytical diffractometer with CuKα radiation operated at 45 kV and 40 mA. Samples were scanned from 5 to 70°2θ with a step size of 0.0167°2θ using a X'Celerator detector. The equivalent time per step was 30 s, resulting in a total measurement time of 15 min per scan. Rutile was used as external standard.

The chemical shrinkage was measured by continuously monitoring the position of an oil drop in a capillary on top of a sealed container of 7 g of cement paste (6-mm height) covered by water. The experiments were carried out in a bath at a constant temperature of 20 °C. The experiments were repeated 3 times for each sample. A blank sample filled with quartz and water was used to isolate the shrinkage of the cementitious blends only. The signal of the quartz system was subtracted to the signal of the systems.

3.3. Porosity

For MIP measurements, dried samples were tested. All experiments were carried out using Porotec 140 and 440 devices. 0.7 g (2 pieces) of paste was used for each experiment. A contact angle of 120° was used since a better agreement was found with the pore size obtained by ¹H NMR using this value [31].

4. Results and discussion

4.1. Comparison of hydration between grey and white cement

The hydration study was carried out on both grey and white cement to check if the hydration is similar. Fig. 1 shows the microstructure observed by SEM of PC and LC³-50 (95.0%) using grey cement and WPC and WLC³-50 (95.0%) with white cement at 3 days of hydration. No significant differences are observed, except the absence of iron-bearing phase in the microstructure of white cement systems. A much denser microstructure is observed for the blends compared with plain cement.

The degree of hydration of clinker is shown in Fig. 2(a). The WPC system has a slightly higher DoH at late ages, which can be due to the absence of the low-reactive ferrite phase in the clinker. Moreover, the slowing down of clinker hydration from 3 days onwards observed for the LC³-50 (95.0%) detailed in [32] is also measured using white cement in the WLC³-50 (95.0%) blend. Portlandite content is shown in Fig. 2(b). The portlandite consumption for the pozzolanic reaction is slightly delayed for the W LC³-50 (95.0%), but the evolution is similar.

4.2. C-A-S-H composition

Fig. 3 shows the comparison of SEM-EDS and STEM-EDS results for the PC and the LC³-50 systems. The Al/Ca and Si/Ca atomic ratios are plotted to better identify the C-A-S-H composition and to exclude the phases intermixed with C-A-S-H. For SEM-EDS, the C-A-S-H composition is defined at the right edge of the cloud of points collected, corresponding to the least intermixed C-A-S-H. Globally, a good agreement is found between the two techniques, considering the error of measurement. The deviations observed for STEM-EDS can be explained by the absence of a standard database for the measurements, as well as the inhomogeneities of the sample thickness. For SEM-EDS, the intermixing with other phases is the main reason for the error in the determination of the C-A-S-H composition, especially for the LC³-50 (95.0%) system.

Table 4 summarizes the Al/Ca and Si/Ca atomic ratios obtained for the different systems using both SEM-EDS and STEM-EDS techniques. Similar aluminium incorporation is observed for the reference PC and the LC³-50 (17.0%). The aluminium incorporation in C-A-S-H significantly increases with the calcined kaolinite content of the calcined clay. According to [32], this increase of aluminium incorporation is due to the increase of the aluminium concentration of the pore solution with the increase of the calcined kaolinite content. The Si/Ca ratio is higher for the LC³-50 blends than for PC. This can be explained by the pozzolanic reaction of the metakaolin in the calcined clay, providing aluminium and silicon to the system. This leads to the consumption of portlandite and a decrease of the calcium concentration in the pore solution [33]. It seems that the Si/Ca ratio also increases with the calcined kaolinite content for STEM-EDS results. However, this is not really observed by SEM-EDS.

As a comparison, the C-A-S-H composition of the white cement systems is also given in Table 4. Similar results are obtained between PC
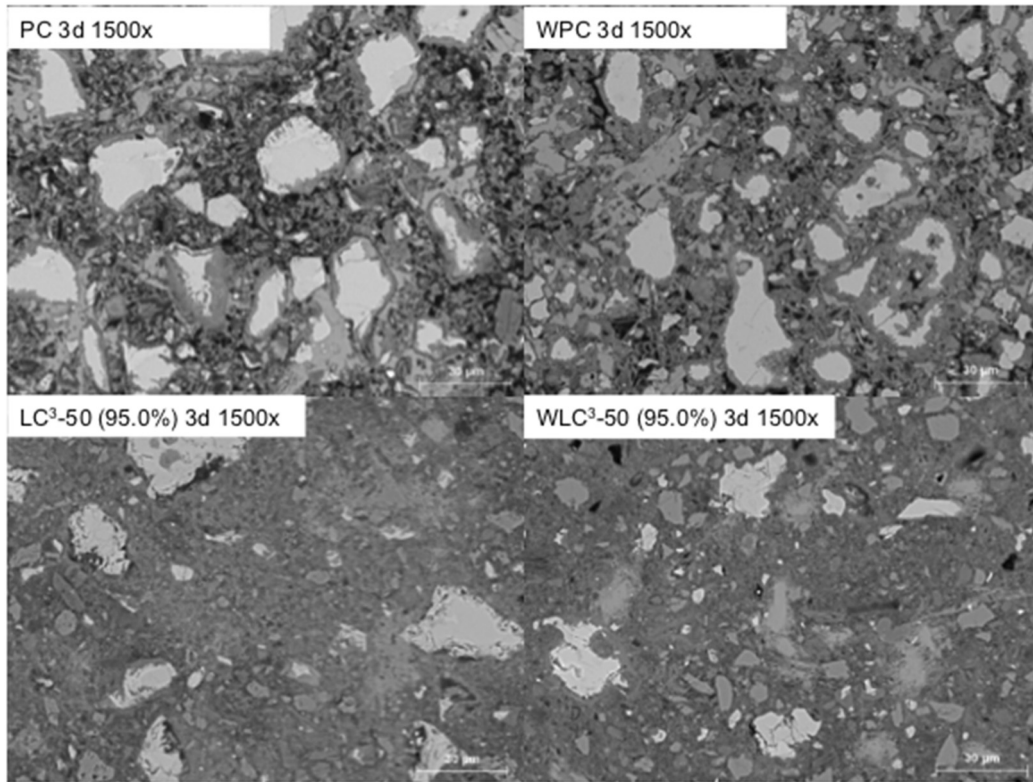
Fig. 1. Microstructure of PC and LC³-50 (95.0%) blend using grey cement and WPC and WLC³-50 (95.0%) with white cement at 3 days of hydration.

and WPC systems, and between LC³-50 and WLC³-50 blends, for a similar calcined kaolinite content.

4.3. C-A-S-H morphology

The microstructure of PC and the LC³-50 (17.0%), (50.3%) and (95.0%) blends is shown in Bright Field (BF) mode and in High Angle Annular Dark Field (HAADF) mode in Fig. 4 (PC and LC³-50 (17.0%)) and in Fig. 5 (LC³-50 (50.3%) and LC³-50 (95.0%)). In all systems, a fibrillar C-A-S-H morphology is observed. Thus, neither the reaction of the calcined clay nor the calcined kaolinite content of the calcined clay influences the morphology of C-A-S-H. In addition to C-A-S-H, ettringite (AFt) is also observed in the LC³-50 (17.0%), as well as unreacted

metakaolin in LC³-50 (95.0%).

4.4. Density of C-A-S-H

4.4.1. Adsorption of water on metakaolin particles

A preliminary test was carried out to investigate the influence of the water adsorption on metakaolin particles, a mix of calcined clay with 95.0% of calcined kaolinite and water with the same water to calcined clay ratio as for the WLC³-50 blends was studied. Fig. 6 shows the CPMG signal for this sample. It shows that 97.5% of water is present as free water in pores as large as capillary pores detected 30 min after casting for WPC and WLC³-50 blends. Only a minor part of the signal is detected in pores showing similar relaxation time as spins in gel and
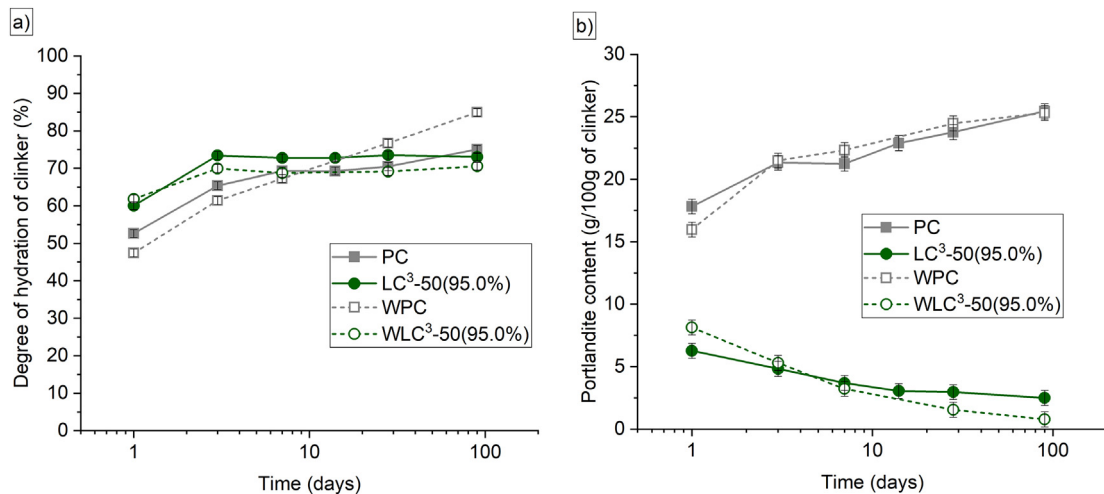
Fig. 2. Clinker hydration degree (a) and portlandite content (b) for PC and LC³-50 (95.0%) blend using grey cement [32] and WPC and WLC³-50 (95.0%) with white cement.
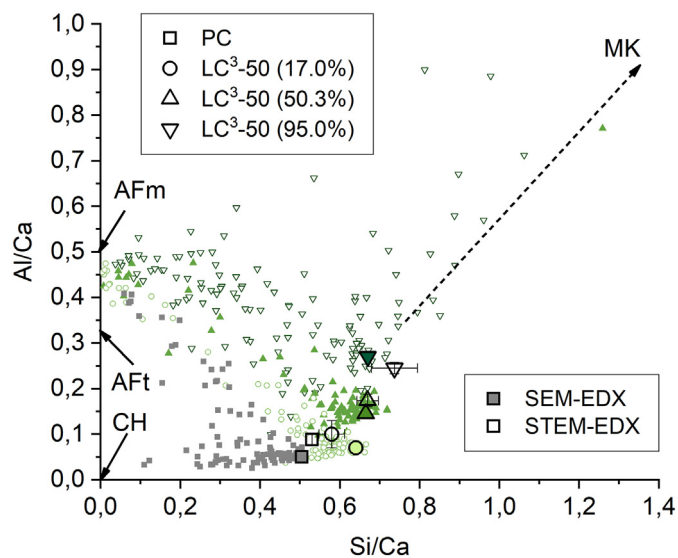
Fig. 3. C-A-S-H composition for PC and LC^3-50 (17.0%), (50.3%) and (95.0%) at 28 days of hydration obtained by SEM-EDS (cloud of points and least inter-mixed composition) [32] and STEM-EDS.

Table 4
Al/Ca and Si/Ca atomic ratios of C-A-S-H obtained by SEM-EDS and STEM-EDS.

	SEM-EDS		STEM-EDS	
	Al/Ca	Ca/Si	Al/Ca	Ca/Si
PC	0.06 ± 0.01	1.96 ± 0.06	0.08 ± 0.01	1.89 ± 0.10
LC^3-50 (17.0%)	0.07 ± 0.02	1.61 ± 0.05	0.08 ± 0.03	1.75 ± 0.08
LC^3-50 (50.3%)	0.13 ± 0.02	1.49 ± 0.05	0.16 ± 0.01	1.54 ± 0.07
LC^3-50 (95.0%)	0.26 ± 0.03	1.49 ± 0.10	0.24 ± 0.01	1.37 ± 0.12

	SEM-EDS	
	Al/Ca	Ca/Si
WPC	0.05 ± 0.01	1.85 ± 0.06
WLC^3-50 (23.8%)	0.12 ± 0.01	1.61 ± 0.03
WLC^3-50 (39.0%)	0.17 ± 0.02	1.61 ± 0.06
WLC^3-50 (47.5%)	0.19 ± 0.04	1.56 ± 0.13
WLC^3-50 (95.0%)	0.28 ± 0.02	1.56 ± 0.08

interlayer water of C-A-S-H. No solid signal was detected using QE pulse sequence. In Fig. 6, it is also shown the signal of the clay stored at 100% relative humidity, until reaching stable mass of the wet powder. A very small amount of water is adsorbed by the metakaolin particles. A mass increase of only 2.8% was measured with most of this mass increase (about 80%) with similar relaxation time to interlayer water. In LC^3-50 blends, the mass fraction of metakaolin is much lower than for the clay sample stored at 100% RH. Thus, the influence of the water adsorption on metakaolin particles will have a negligible role on the ^{1}H NMR outputs.

4.4.2. Assignment of ^{1}H NMR signals

The relaxation time spectra at 1 and 28 days of hydration are shown in Fig. 7 (a) for WPC and WLC^3-50 (39.0%) and (95.0%). The coloured boxes indicate the range of relaxation times for the different water populations corresponding to the water present in the capillaries/interhydrate space, in the gel pores, in the interlayer of the C-A-S-H or bound to crystalline phases. The amount of capillary water decreases with time due to its consumption during hydration. The trend towards smaller relaxation time indicates the decrease of the size of the water filled capillary pores. The C-A-S-H formation is observed through the evolution of gel water and interlayer water. Finally, the formation of

crystalline phases also increases with time. For WLC^3-50 blends, the size of the **water filled** capillary pores appears to be larger than for the WPC at 28 days, even though MIP measurements in Fig. 9 show a lower breakthrough diameter of the capillary porosity. This is because more of the mixing water is consumed in the plain WPC system; the higher amount of capillary water remaining in the WLC3-50 systems, means that pores are filled to larger sizes.

Based on the quantification of the different peaks in Fig. 7(a), the evolution of the different water populations is shown in Fig. 7(b), (c) and (d). For WPC in Fig. 7(b), the amount of capillary water rapidly decreases to reach 45% of the total water signal at 1 day and 20% at 7 days. This amount keeps decreasing with time to be close to 3% at 150 days of hydration. The amounts of interlayer and gel water keep increasing with time, as well as the amount of water bound to crystalline phases. By comparison, the results obtained by Müller are indicated by plain lines [24]. The differences can be attributed to the extra sulfate and alkali added to the cement in this study. The lower amount of gel water at early age is likely to be due to the sulfate adjustment of the cement, as observed in [34].

For the WLC^3-50 (95.0%) in Fig. 7(c), the amount of capillary water is constant with time from 1.5 days onwards. About 43% of the total water signal is still present in the capillaries from 1 day onwards and the average capillary water left after 1.5 days is about 33%. The amount of water present in the gel pores reaches a maximum of about 36% of the total water signal at approximately 1.5 days of hydration. This amount slightly decreases then to 26% after 200 days of hydration. After 1.5 days, the interlayer water signal keeps increasing. The decrease of the gel to interlayer water ratio from 1.5 days onwards is thought to be due to the formation of inner "denser" C-A-S-H. Concerning the signal fraction of the water bound to crystalline phases, a decrease could have been expected with time due to the pozzolanic reaction of the metakaolin from calcined clay with portlandite. However, this decrease is not observed even if the intensity of the peak is slightly lower than for WPC at late ages. This is explained first by the formation of carboaluminate hydrates in WLC^3-50 blends, and also because the fraction of water bound in portlandite (0.24 g of water per g of portlandite) is lower than ettringite (0.45 g of water per g of ettringite). Thus, the amount of ettringite plays a bigger role in the peak intensity than portlandite.

The influence of the calcined kaolinite content is shown for the WLC^3-50 (39.0%) blend in Fig. 7(d). The main difference with the WLC^3-50 (95.0%) is that the stabilization of the capillary water content occurs at around 7 days and its amount is lower (27% of the total water signal). Thus, less water is present in the capillaries. The maximum amount of gel water is measured at around 5 days of hydration and decreases then, whereas the amount of interlayer water keeps increasing with time. The signal of the water bound to crystalline phases keeps slightly increasing with time.

4.4.3. Bulk and solid density of C-A-S-H

The values of solid and bulk density of C-A-S-H were determined according to the method described in Supplementary material. Results are shown in Fig. 8 for WPC and for the different WLC^3-50 blends. Based on a sensitivity analysis, the error for the determination of the solid and bulk density is ± 0.18 g·cm^{-3} and ± 0.07 g·cm^{-3}, respectively. The solid density of C-A-S-H (excluding gel water) slightly decreases from about 2.9 g·cm^{-3} to 2.7 g·cm^{-3} from 1 to 28 days of hydration. There is a spread between the different systems but the variations are in the range of error. Thus, there is no major change in C-A-S-H solid density for reference WPC and for the WLC^3-50 blends. The slight decrease of the solid density observed with time for all systems can be explained by the increase of the C-A-S-H layers with time [24]. The water present at C-A-S-H surface is in direct contact with the gel water and shows a longer relaxation time than the interlayer water. For a number n of calcium silicate layers, n-1 interlayers of water are detected by ^{1}H NMR. Thus, with the increase of the number of layers n of
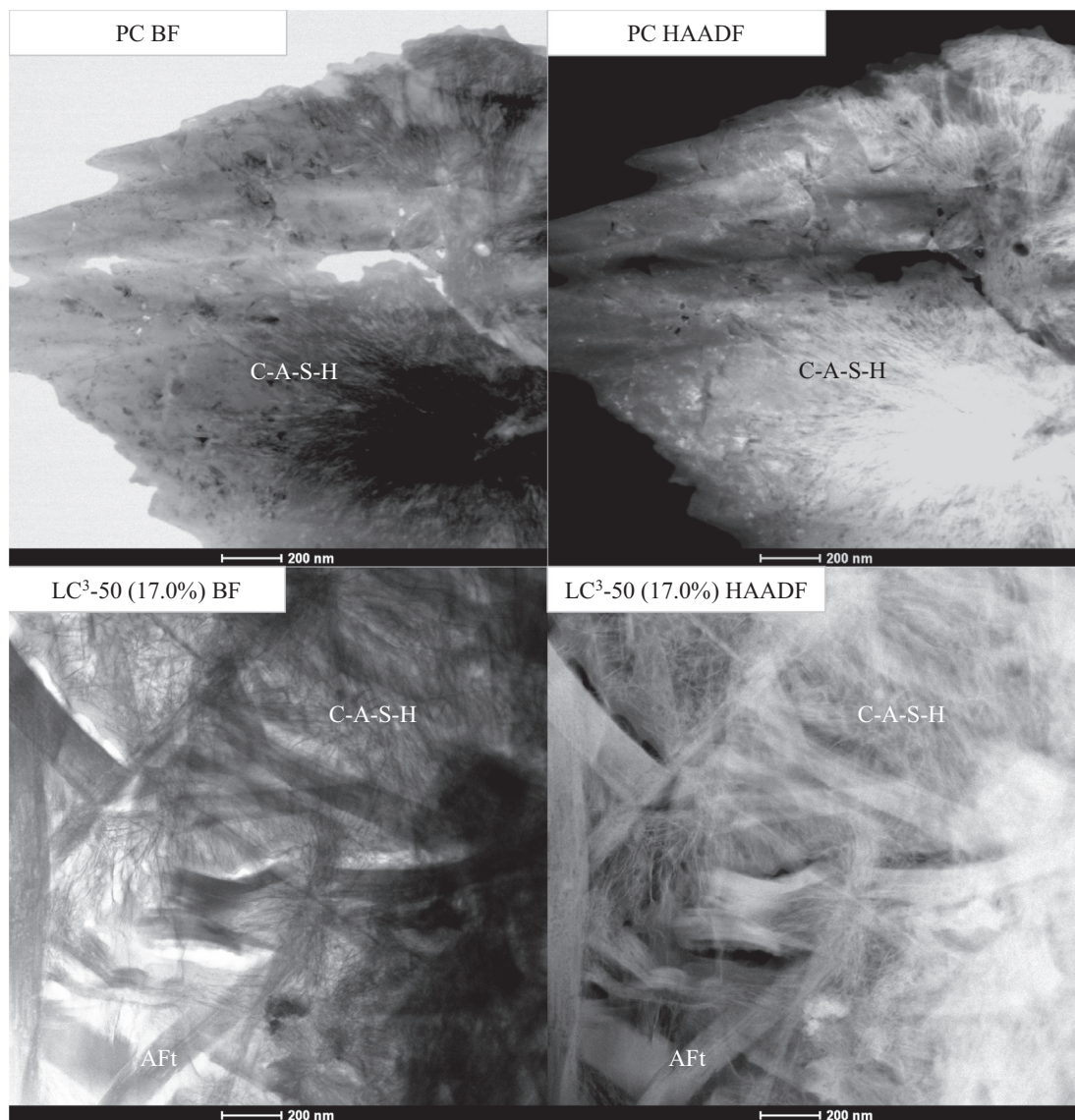
Fig. 4. Microstructure of PC and LC³-50 (17.0%) at 28 days of hydration in Bright Field (BF) and High Angle Annular Dark Field (HAADF) modes. AFt refers to ettringite.

the C-A-S-H, the average solid density slightly decreases since the ratio n/n − 1 decreases with n.

The determination of the bulk density of C-A-S-H (including gel water) also shows very similar results for WPC and for WLC³-50 blends. The values globally slightly increase from $1.85 \, g \cdot cm^{-3}$ at 1 day to $1.92 \, g \cdot cm^{-3}$ at 28 days of hydration. The small variations observed between the different systems are in the range of error. Thus, neither the calcined clay nor the calcined kaolinite content of the calcined clay impacts the density of C-A-S-H significantly. The slight increase in density with time observed for all systems corresponds to the densification of the C-A-S-H, with the slowing down/stopping of gel pore formation from 1 to 7 days depending on the system. Similar results were found by Muller [27] for a blend with 10% of silica fume.

4.5. Porosity investigation: comparison between MIP and NMR data

The MIP results obtained at 3 days and 28 days of hydration for WPC and the different WLC³-50 blends are shown in Fig. 9(a) and (b). At 3 days of hydration, a significant refinement of pore connectivity is observed for the WLC³-50 (47.5%) and (95.0%) blends compared with PC, with a lower pore threshold radius. However, these three systems

show the same total porosity value. At 28 days of hydration, the reference WPC has the lowest total porosity. All blends however present a refinement of pore connectivity compared with PC, this refinement increasing with the calcined kaolinite content of the calcined clay. Fig. 10(a) and (b) shows the derivative of the MIP cumulative curves. A peak corresponding to capillary porosity can be observed for each sample. However, contrary to the study of Muller [31], it is not possible to clearly distinguish a second peak corresponding to the gel porosity of C-A-S-H. For the WLC³-50 blends, the capillary peak is shifted towards lower pore entry radius.

In his work, Müller got excellent correlation between MIP and ¹H NMR capillary porosity. In this study, since it is not possible to distinguish the capillary from the gel pore peak, the approach consists of comparing the capillary pore volume based on ¹H NMR measurements and the void formation (from chemical shrinkage) to the MIP data. From the results obtained by ¹H NMR in Fig. 7 and chemical shrinkage, the volume of capillary and gel porosity can be measured according to Eqs. (1)–(3), considering the gel water I_{gel}, the water-filled capillaries I_{cap} and the capillary voids formed due to chemical shrinkage and self-desiccation I_{void}. w/b refers to the water to binder ratio and V_{paste} is the volume of paste per gram of anhydrous binder.
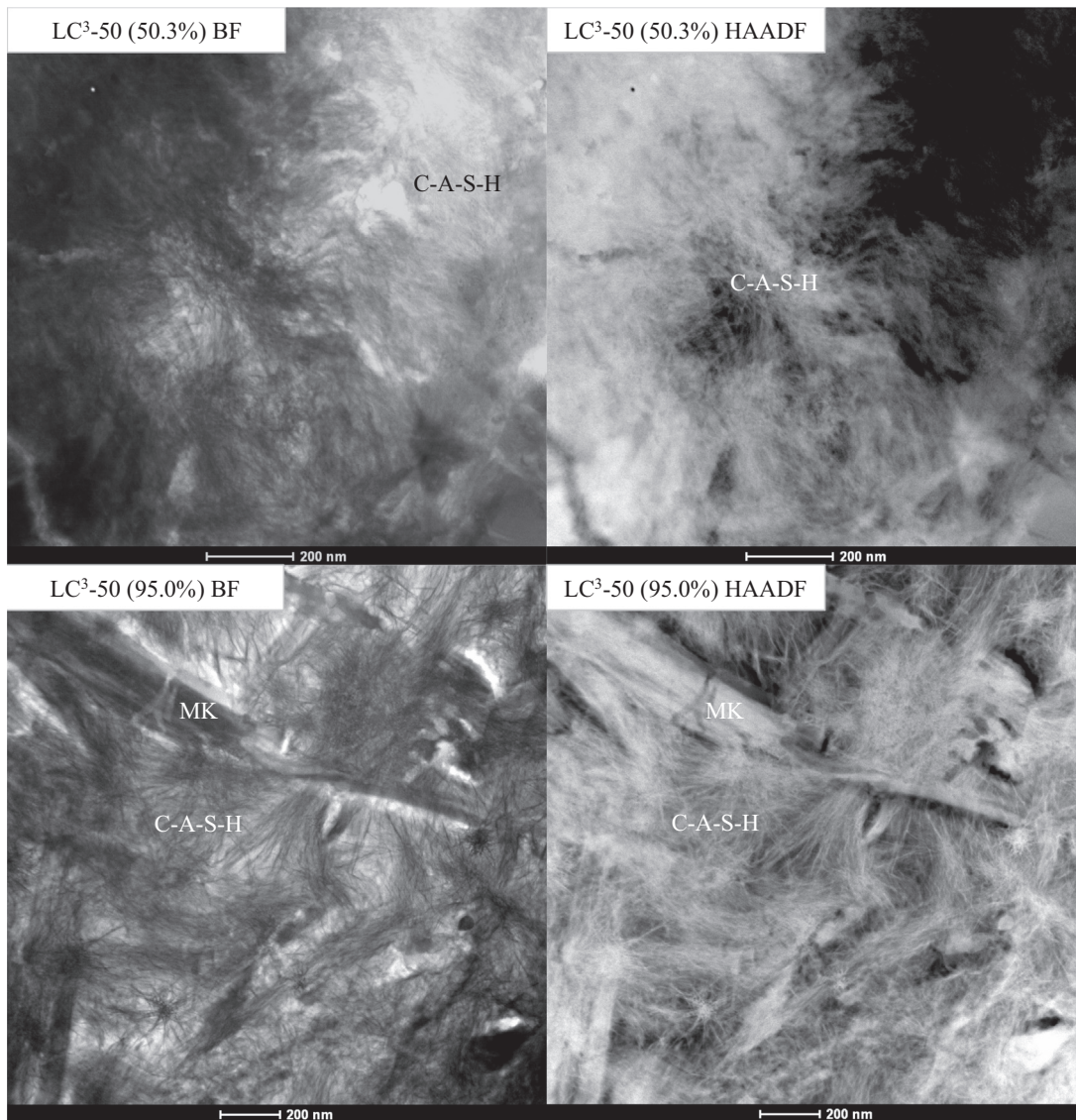
Fig. 5. Microstructure of LC³-50 (50.3%) and (95.0%) at 28 days of hydration Bright Field (BF) and High Angle Annular Dark Field (HAADF) modes. MK refers to unreacted metakaolin particle.
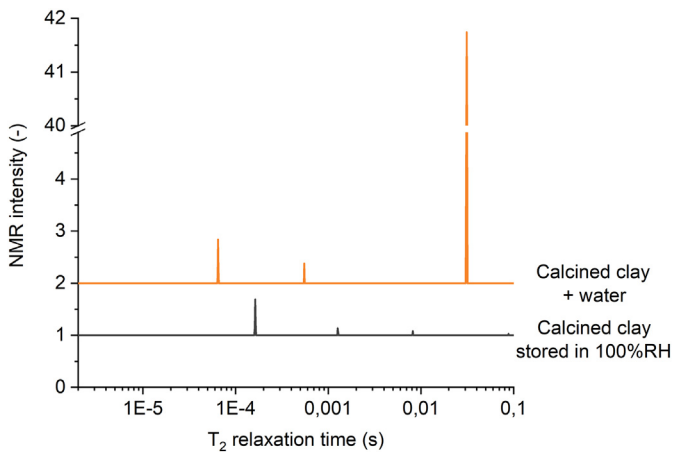
Fig. 6. T₂ distribution for calcined clay–water mix and calcined clay stored at 100% of relative humidity.

$$V_{capillary\ voids} = I_{void} \times \frac{w/b}{V_{paste}} \tag{1}$$

$$V_{capillary\ water} = I_{cap} \times \frac{w/b}{V_{paste}} \tag{2}$$

$$V_{gel\ pores} = I_{gel} \times \frac{w/b}{V_{paste}} \tag{3}$$

Fig. 11(a) and (b) shows the volume occupied by the capillary and gel pores in the WPC and the different WLC³-50 blends at 3 days and 28 days of hydration. The total porosity obtained by MIP is also shown and compared to the results obtained by ¹H NMR. From the comparison, it appears that mercury penetrates all capillary pores and reaches some of gel pores. The fraction of gel pores reached by MIP varies between the different systems. About half of gel pores are reached by MIP for the plain cement system at 28 days of hydration. For WLC³-50 blends, the volume of mercury-filled gel pores decreases with the increase of the calcined kaolinite content. As observed by MIP in Figs. 9–10, a significant refinement of pore connectivity is observed for the blends, this refinement increasing with the calcined kaolinite content of the calcined clay. If the connectivity is finer, it might become
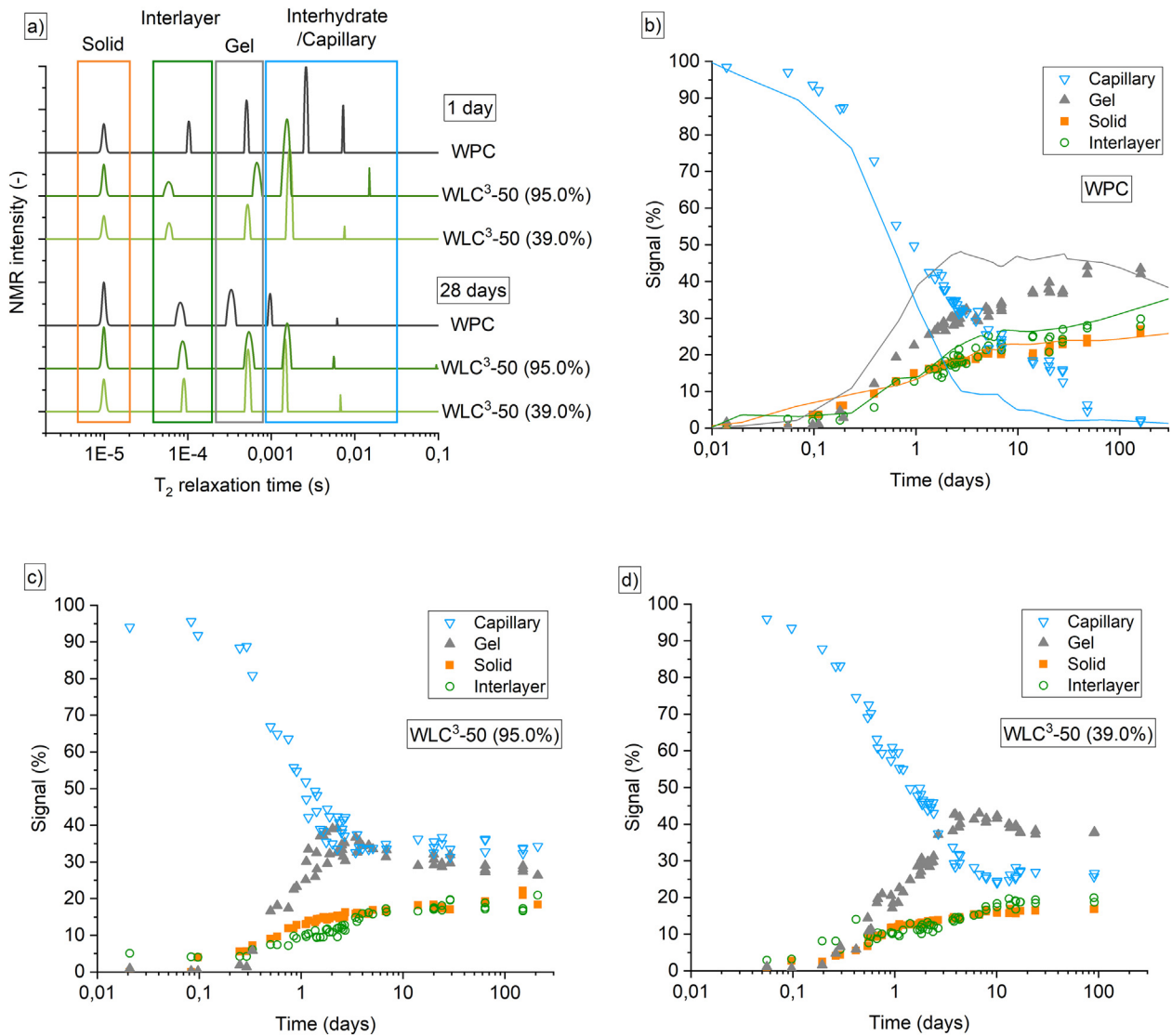
Fig. 7. (a) Relaxation time for WPC and WLC³-50 (39.0%) and (95.0%) at 1 and 28 days of hydration. (b) Evolution of the different NMR signal fractions for WPC. Plain lines indicate Müller's data for WPC [24]. (c) and (d) NMR signal fractions for WLC³-50 (95.0%) and (39.0%).
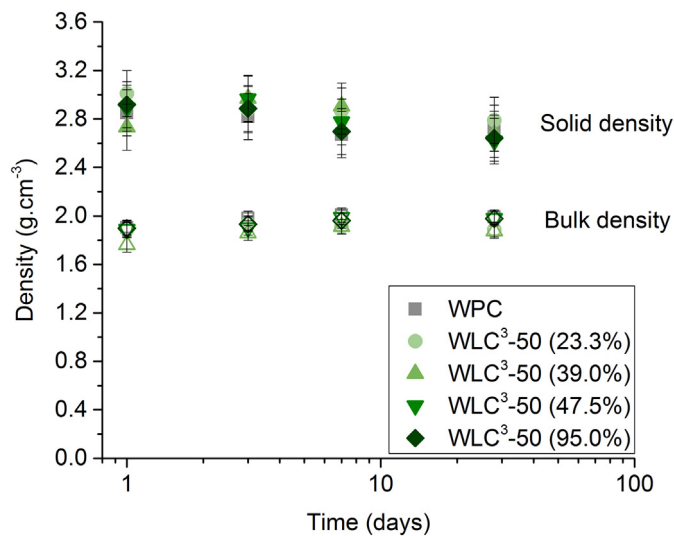
Fig. 8. C-A-S-H density for WPC and WLC³-50 blends: plain and hollow symbols show the solid and bulk density, respectively.

harder for the mercury to intrude the C-A-S-H gel pores. This could explain why the fraction of gel pores intruded by mercury decreases with the increase of the calcined kaolinite content.

5. Conclusion

The C-A-S-H of LC³-50 systems show significant changes in terms of composition. The aluminium incorporation increases with the calcined kaolinite content of the calcined clay. The silicon to calcium ratio is quite similar for all blends, but higher than plain cement. A good agreement was found between SEM-EDS and STEM-EDS. Use of STEM overcomes the issue of interaction volume and phase mixing in the SEM. However, larger scatter was found using STEM. Due to its much easier sample preparation, SEM-EDS is much more practical and more accessible way to obtain the composition of the C-A-S-H.

In terms of morphology, STEM provides unique information on the morphology of the C-A-S-H, where a fibrillar morphology is observed for all systems. There is no significant influence of the calcined clay or of the calcined kaolinite of the calcined clay on the C-A-S-H morphology.

The density of C-A-S-H investigated by ¹H NMR also shows that there is no significant influence of the calcined kaolinite content of the
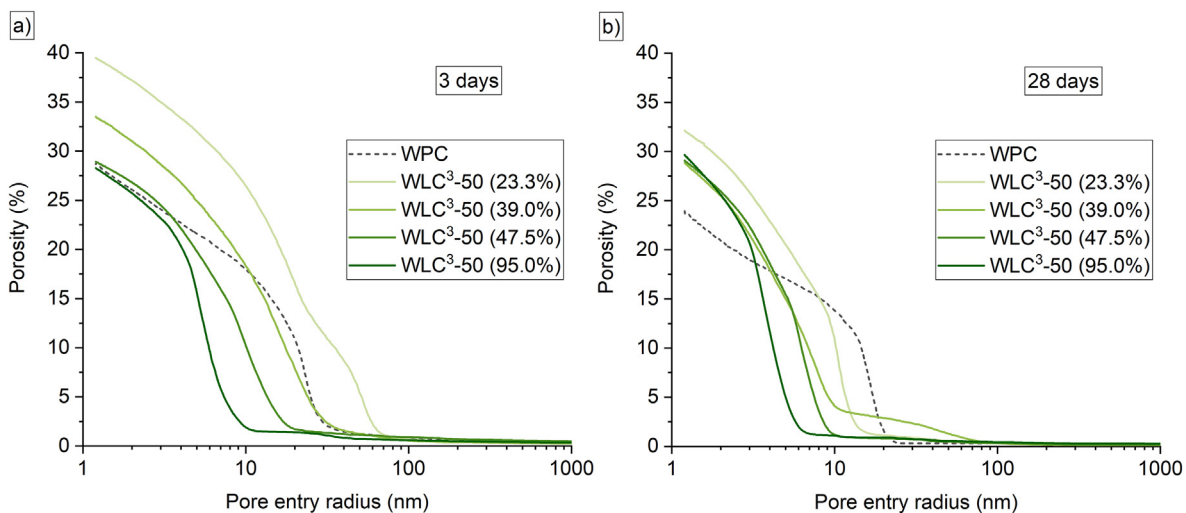
Fig. 9. MIP results at 3 and 28 days of hydration for WPC and WLC^3-50 blends.
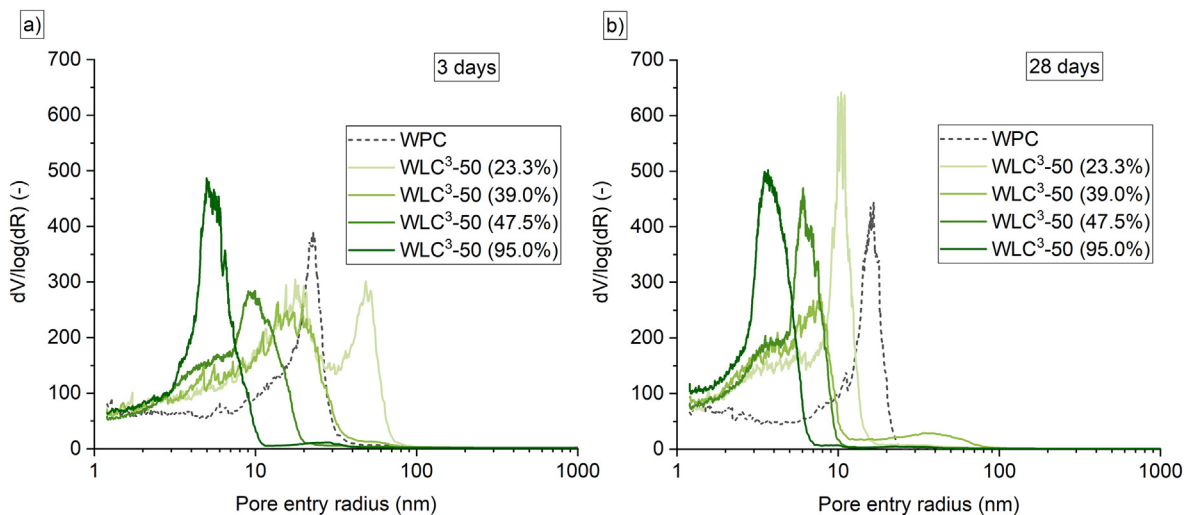
Fig. 10. MIP derivative curves at 3 and 28 days of hydration for WPC and WLC^3-50 blends.
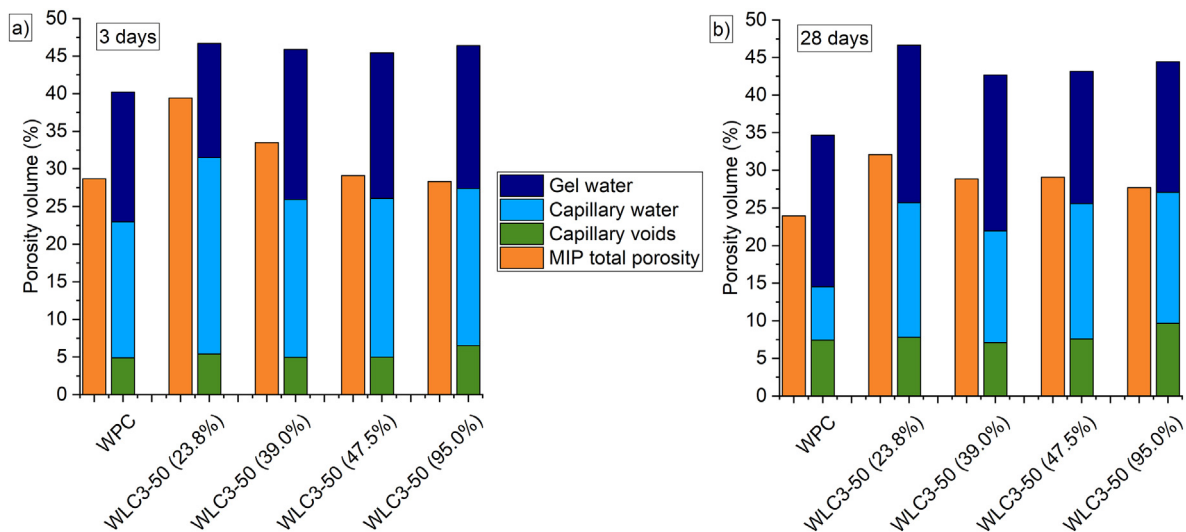
Fig. 11. Comparison between MIP porosity and ^{1}H NMR combined with chemical shrinkage outputs at 3 days (a) and 28 days (b) of hydration.

density of C-A-S-H. A solid density of around 2.8 g·cm^{-3} is found, and a bulk density of 1.9 g·cm^{-3} is determined for all systems at 28 days of hydration.

In parallel to the determination of the C-A-S-H density, ^{1}H NMR provides new insights on WLC^3-50 hydration. After the slowing down of clinker hydration at 3 days of hydration, the amount of interlayer water keeps increasing, indicating continuing formation of C-A-S-H. This is due to the on-going reaction of metakaolin, indicated by the portlandite consumption, and the change in C-A-S-H composition.

^{1}H NMR also provides a better understanding of the porosity results obtained by MIP, Mercury fully penetrates capillary pores, and part of gel pores. The fraction of gel pores reached by MIP decreases with the increase of the calcined kaolinite content of the calcined clay.

Acknowledgements

Supplementary data

Supplementary data to this article can be found online at https://doi.org/10.1016/j.cemconres.2018.10.011.

References

[1] E. L'Hôpital, B. Lothenbach, G. Le Saout, et al., Incorporation of aluminium in calcium-silicate-hydrates, Cem. Concr. Res. 75 (2015) 91–103, https://doi.org/10.1016/j.cemconres.2015.04.007.

[2] H.F.W. Taylor, Cement Chemistry, 2nd edition, (1997).

[3] Bazzoni, A Study of Early Hydration Mechanisms of Cement by Means of Electron Microscopy, EPFL PP - Lausanne (2014).

[4] J.E. Rossen, K.L. Scrivener, Optimization of SEM-EDS to determine the C–A–S–H composition in matured cement paste samples, Mater. Charact. 123 (2017) 294–306, https://doi.org/10.1016/j.matchar.2016.11.041.

[5] Z. Dai, T.T. Tran, J. Skibsted, Aluminum incorporation in the C-S-H phase of white portland cement-metakaolin blends studied by 27 Al and 29 Si MAS NMR spectroscopy, J. Am. Ceram. Soc. 97 (2014) 2662–2671, https://doi.org/10.1111/jace.13006.

[6] P.T. Durdziński, M. Ben Haha, M. Zajac, K.L. Scrivener, Phase assemblage of composite cements, Cem. Concr. Res. 99 (2017) 172–182, https://doi.org/10.1016/j.cemconres.2017.05.009.

[7] F. Deschner, F. Winnefeld, B. Lothenbach, et al., Hydration of Portland cement with high replacement by siliceous fly ash, Cem. Concr. Res. 42 (2012) 1389–1400, https://doi.org/10.1016/j.cemconres.2012.06.009.

[8] K. De Weerdt, Haha M. Ben, G. Le Saout, et al., Hydration mechanisms of ternary Portland cements containing limestone powder and fly ash, Cem. Concr. Res. 41 (2011) 279–291, https://doi.org/10.1016/j.cemconres.2010.11.014.

[9] V. Kocaba, Development and Evaluation of Methods to Follow Microstructural Development of Cementitious Systems Including Sl, EPFL PP - Lausanne. (2009).

[10] I.G. Richardson, G.W. Groves, Microstructure and microanalysis of hardened ordinary Portland cement pastes, J. Mater. Sci. 28 (1993) 265–277, https://doi.org/10.1007/BF00349061.

[11] B. Lothenbach, F. Winnefeld, C. Alder, et al., Effect of temperature on the pore solution, microstructure and hydration products of Portland cement pastes, Cem. Concr. Res. 37 (2007) 483–491, https://doi.org/10.1016/j.cemconres.2006.11.016.

[12] F. Deschner, B. Lothenbach, F. Winnefeld, J. Neubauer, Effect of temperature on the hydration of Portland cement blended with siliceous fly ash, Cem. Concr. Res. 52 (2013) 169–181, https://doi.org/10.1016/j.cemconres.2013.07.006.

[13] K. Scrivener, R. Snellings, B. Lothenbach, A Practical Guide to Microstructural Analysis of Cementitious Materials, CRC Press, 2016.

[14] H.F.W. Taylor, J.W. Howison, Relationships between calcium silicates and clay minerals, Clay Miner. Bull. 3 (1956) 98–111.

[15] A. Nonat, The structure and stoichiometry of C-S-H, Cem. Concr. Res. 34 (2004) 1521–1528, https://doi.org/10.1016/j.cemconres.2004.04.035.

[16] B. Lothenbach, A. Nonat, Calcium silicate hydrates: solid and liquid phase composition, Cem. Concr. Res. 78 (2015) 57–70, https://doi.org/10.1016/j.cemconres.2015.03.019.

[17] M.D. Andersen, H.J. Jakobsen, J. Skibsted, Characterization of white Portland cement hydration and the C-S-H structure in the presence of sodium aluminate by27Al and29Si MAS NMR spectroscopy, Cem. Concr. Res. 34 (2004) 857–868, https://doi.org/10.1016/j.cemconres.2003.10.009.

[18] M.D. Andersen, H.J. Jakobsen, J. Skibsted, Incorporation of aluminum in the calcium silicate hydrate (C−S−H) of hydrated Portland cements: a high-field 27Al and 29Si MAS NMR investigation, Inorg. Chem. 42 (2003) 2280–2287, https://doi.org/10.1021/ic020607b.

[19] I. Richardson, G. Groves, The structure of the calcium silicate hydrate phases present in hardened pastes of white Portland cement/blast-furnace slag blends, J. Mater. Sci. 32 (1997) 4793–4802, https://doi.org/10.1023/A:1018639232570.

[20] C.A. Love, I.G. Richardson, A.R. Brough, Composition and structure of C-S-H in white Portland cement-20% metakaolin pastes hydrated at 25 °C, Cem. Concr. Res. 37 (2007) 109–117, https://doi.org/10.1016/j.cemconres.2006.11.012.

[21] M. Antoni, J. Rossen, F. Martirena, K. Scrivener, Cement substitution by a combination of metakaolin and limestone, Cem. Concr. Res. 42 (2012) 1579–1589.

[22] J.E. Rossen, Stability of C-A-S-H in Pastes of Alite and Cement Blended With Supplementary Cementitious Materials, (2014), p. 172, https://doi.org/10.5075/epfl-thesis-6294.

[23] I.G. Richardson, The nature of C-S-H in hardened cements, Cem. Concr. Res. 29 (1999) 1131–1147, https://doi.org/10.1016/S0008-8846(99)00168-4.

[24] Muller AC, K.L. Scrivener, A.M. Gajewicz, P.J. Mcdonald, Densification of C–S–H measured by 1H NMR relaxometry, J. Phys. Chem. (2012) 1–43, https://doi.org/10.1021/jp3102964.

[25] A.C.A. Muller, K.L. Scrivener, A.M. Gajewicz, P.J. McDonald, Use of bench-top NMR to measure the density, composition and desorption isotherm of C-S-H in cement paste, Microporous Mesoporous Mater. 178 (2013) 99–103, https://doi.org/10.1016/j.micromeso.2013.01.032.

[26] F. Avet, R. Snellings, A. Alujas Diaz, et al., Development of a new rapid, relevant and reliable (R3) test method to evaluate the pozzolanic reactivity of calcined kaolinitic clays, Cem. Concr. Res. 85 (2016) 1–11, https://doi.org/10.1016/j.cemconres.2016.02.015.

[27] A.C.A. Muller, Characterization of Porosity & C-S-H in Cement Pastes by ^{1}H NMR, EPFL PP - Lausanne (2014).

[28] S.L. Poulsen, V. Kocaba, G. Le Saoût, et al., Improved quantification of alite and belite in anhydrous Portland cements by29Si MAS NMR: effects of paramagnetic ions, Solid State Nucl. Magn. Reson. 36 (2009) 32–44, https://doi.org/10.1016/j.ssnmr.2009.05.001.

[29] J. Zhang, G.W. Scherer, Comparison of methods for arresting hydration of cement, Cem. Concr. Res. 41 (2011) 1024–1036, https://doi.org/10.1016/j.cemconres.2011.06.003.

[30] L. Konecny, S.J. Naqvi, The effect of different drying techniques on the pore size distribution of blended cement mortars, Cem. Concr. Res. 23 (1993) 1223–1228, https://doi.org/10.1016/0008-8846(93)90183-A.

[31] A.C.A. Muller, K.L. Scrivener, A reassessment of mercury intrusion porosimetry by comparison with1H NMR relaxometry, Cem. Concr. Res. 100 (2017) 350–360, https://doi.org/10.1016/j.cemconres.2017.05.024.

[32] F. Avet, K. Scrivener, Investigation of the calcined kaolinite content on the hydration of Limestone Calcined Clay Cement (LC3), Cem. Concr. Res. 107 (2018) 124–135, https://doi.org/10.1016/j.cemconres.2018.02.016.

[33] B. Lothenbach, K. Scrivener, R.D. Hooton, Supplementary cementitious materials, Cem. Concr. Res. 41 (2011) 1244–1256, https://doi.org/10.1016/j.cemconres.2010.12.001.

[34] E.M.J. Berodier, Impact of the Supplementary Cementitious Materials on the Kinetics and Microstructural Development of Cement Hydration, EPFL PP - Lausanne (2015).